Electronic Supplementary Material (ESI) for Physical Chemistry Chemical Physics.

Supplementary Information

Photoswitching of arylazopyrazoles upon S1 (nπ*) excitation studied by transient absorption and ab-initio molecular dynamics

Till Reichenauer[1#], Marcus Böckmann[2#], Katharina Ziegler[3], Vikas Kumar[1],

Bart Jan Ravoo[3]*, Nikos Doltsinis[2]*, Sebastian Schlücker[1]*

[1] Physical Chemistry I and Center for Nanointegration Duisburg-Essen (CENIDE, Universität Duisburg-Essen, 45141 Essen, Germany)

[2] Institute of Solid-State Theory and Center for Soft Nanoscience (SoN), Westfälische Wilhelms-Universität Münster, 48149 Münster, Germany

[3] Organic Chemistry Institute and Center for Soft Nanoscience (SoN), Westfälische Wilhelms-Universität Münster, D-48149 Münster, Germany;

[#]These authors contributed equally

*Corresponding authors: b.j.ravoo@uni-muenster.de; nikos.doltsinis@uni-muenster.de; sebastian.schluecker@uni-due.de

1. Synthesis of the AAPs

The presented molecules have been previously documented in literature and analyzed by Ravoo and colleagues, specifically in terms of their photochemical characteristics, photoisomerization quantum yields, photostationary states (PSS), and *Z*-isomer half-life times.

General procedure I: Synthesis of 3-(2-phenylhydrazono)pentane-2,4- diones[1]

The chemical reaction was carried out by adding $NaNO_2$ (1.2 eq.) dissolved in a small amount of water dropwise to a solution of aniline (1.0 eq.) in AcOH (1.5 mL/mmol) and HCl (12 M, 0.23 mL/mmol) at 0°C. After stirring for 45 minutes, the resulting diazonium salt was transferred to a suspension of pentane-2,4-dione (1.3 eq.) and NaOAc (3 eq.) in EtOH (1 mL/mmol) and water (0.6 mL/mmol). The mixture was stirred for 1 hour and the resulting yellow precipitate was collected through vacuum filtration. The obtained solid was washed with water and water/EtOH (1:1) and dried under vacuum to yield the desired compound.

3-(2-Phenylhydrazono)pentane-2,4-dione

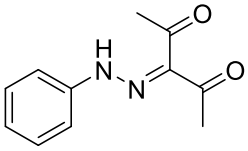

Yield: 8.66 g (42.40 mmol, 80 %) as yellow solid.
^{1}H NMR (300 MHz, $CDCl_3$): δ = 14.74 (s, 1H), 7.45 – 7.38 (m, 4H), 7.20 (ddd, 1H), 2.61 (s, 3H), 2.49 (s, 3H).
ESI-HRMS (MeOH) (m/z): Calculated for $[C_{11}H_{11}N_2O_2]^-$: 203.08260, found 203.08243.

3-(2-(2,6-Dimethylphenyl)hydrazono)pentane-2,4-dione

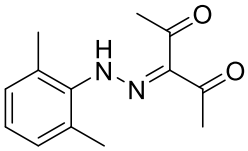

Yield: 3.68 g (15.80 mmol, 79 %) as yellow solid.
^{1}H NMR (300 MHz, $CDCl_3$): δ = 14.98 (s, 1H), 7.14 – 7.07 (m, 3H), 2.63 (s, 3H), 2.46 (s, 6H), 2.41 (s, 3H).
ESI-HRMS (MeOH) (m/z): Calculated for $[C_{13}H_{16}N_2O_2Na]^+$: 255.11036, found 255.11040.

3-(2-(o-Tolyl)hydrazineylidene)pentane-2,4-dione

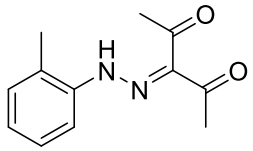

Yield: 8.90 g (40.79 mmol, 87 %) as yellow solid.
^{1}H NMR (300 MHz, $CDCl_3$): δ = 14.96 (s, 1H), 7.74 (dd, J = 8.2, 1.3 Hz, 1H), 7.30 (t, 1H), 7.20 (d, 1H), 7.17 – 7.07 (m, 1H), 2.63 (s, 3H), 2.50 (s, 3H), 2.39 (s, 3H).
ESI-HRMS (MeOH) (m/z): Calculated for $[C_{12}H_{14}N_4H]^+$: 241.0947, found 215.0945.

3-(2-(4-Methoxyphenyl)hydrazono)pentane-2,4-dione

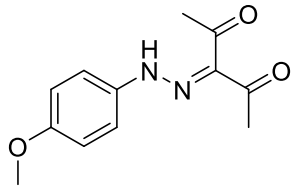

Yield: 5.13 g (21.9 mmol, 88 %) as yellow solid.
^{1}H-NMR (300 MHz, $CDCl_3$): δ = 14.98 (br, 1H, NH), 7.37 (d, *J*HH = 9.1 Hz, 2H, CH), 6.95 (d, *J*HH = 9.1 Hz, 2H, CH), 3.84 (s, 3H, CH3), 2.60 (s, 3H, CH3), 2.48 (s, 3H, CH3).
ESI-HRMS (MeOH) (m/z): Calculated for $[C_{12}H_{14}N_2O_3Na]^+$: 257.0897, found: 257.0910.

General procedure II: Synthesis of AAPs [1]

Hydrazine x hydrate (1 equiv) was added to a solution of desired 3-(2-phenylhydrazono)pentane-2,4-dione (1 equiv) or heptane-3,5-dione dissolved in EtOH and heated at reflux for 3 h. Concentration under reduced pressure yielded the resulting AAP without further purification.

(*E*)-3,5-Dimethyl-4-(phenyldiazenyl)-1H-pyrazole

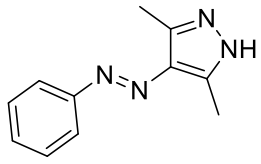

Yield: 7.76 g (38.80 mmol, 92 %) as yellow solid.
^{1}H NMR (300 MHz, $CDCl_3$): δ = 10.15 (s, 1H), 7.85 – 7.75 (m, 2H), 7.53 – 7.43 (m, 2H), 7.43 – 7.35 (m, 1H), 2.63 (s, 6H).
ESI-HRMS (MeOH) (m/z): Calculated for $[C_{11}H_{11}N_4]^-$: 199.09892, found 199.09868.

(*E*)-4-((2,6-Dimethylphenyl)diazenyl)-3,5-dimethyl-1H-pyrazole

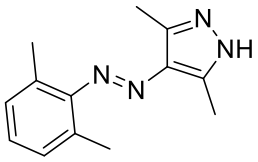

Yield: 3.45 g (15.10 mmol, 95 %) as yellow solid.
^{1}H NMR (300 MHz, $CDCl_3$): δ = 7.14 – 7.09 (m, 3H), 2.57 (s, 6H), 2.37 (s, 6H).
ESI-HRMS (MeOH) (m/z): Calculated for $[C_{13}H_{15}N_4]^-$: 227.13022, found 227.12997.

(*E*)-3,5-Dimethyl-4-(o-tolyldiazenyl)-1H-pyrazole

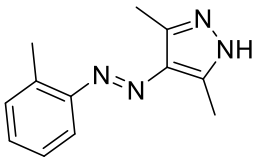

Yield: 5.87 g (27.42 mmol, 92 %) as orange solid.
^{1}H NMR (300 MHz, $CDCl_3$): δ = 7.64 (dd, J = 7.6, 1.6 Hz, 1H), 7.37 – 7.23 (m, 3H), 2.67 (s, 3H), 2.65 (s, 6H).
ESI-HRMS (MeOH) (m/z): Calculated for $[C_{12}H_{14}N_4H]^+$: 215.1291, found 215.1292.

(*E*)-4-((4-Methoxyphenyl)diazenyl)-3,5-dimethyl-1H-pyrazole

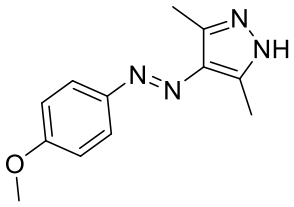

Yield: 2.46 g (10.7 mmol, quantitative) as yellow solid.
^{1}H NMR (300 MHz, CDCl3): δ = 7.79 (m, 2H, CH), 6.98 (m, 2H, CH), 3.88 (s, 3H, OCH3), 2.57 (s, 6H, CH3).
ESI-HRMS (MeOH) (m/z): Calculated for $[C_{12}H_{15}N_4O]^+$: 231.1240, found: 231.1251.

General procedure III: Coupling of arylazopyrazoles to TsO-TEG-OH [1]

The arylazopyrazole (1 eq.) was dissolved in dry ACN. K_2CO_3 (5 eq.), TsO-TEG-OH (1.1 eq.) and LiBr (cat.) were added. The heterogeneous mixture was refluxed for 36 h. Afterwards the solvent was removed under reduced pressure, the resulting residue was dissolved in EtOAc/H_2O (1:1) and the layers were separated. The organic layer was washed with H_2O and brine (2 ×). Then, the organic layer was dried over $MgSO_4$ and the solvent was removed under vacuum. The crude product was purified by column chromatography (SiO_2, DCM/MeOH 97:3).

AAP-1

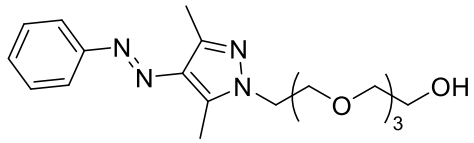

Yield: 1.73 g 4.60 mmol, 92 %) as orange oil.
^{1}H NMR (300 MHz, $CDCl_3$): δ = 7.83 – 7.71 (m, 2H), 7.51 – 7.40 (m, 2H), 7.39 – 7.29 (m, 1H), 4.22 (t, J = 5.4 Hz, 2H), 3.86 (t, J = 5.4 Hz, 2H), 3.74 – 3.65 (m, 3H), 3.64 (d, J = (s, 3H), 2.50 (s, 3H).
^{13}C-NMR (101MHz, $CDCl_3$): δ = 153.62, 142.50, 140.51, 134.98, 129.32, 128.93, 121.77, 77.48, 77.16, 76.84, 72.54, 70.72, 70.60, 70.53, 70.32, 69.91, 61.63, 49.05, 14.18, 9.94.
ESI-HRMS (MeOH) (m/z): Calculated for $[C_{19}H_{28}N_4O_4Na]^+$: 399.20028, found: 399.19994.

AAP-2

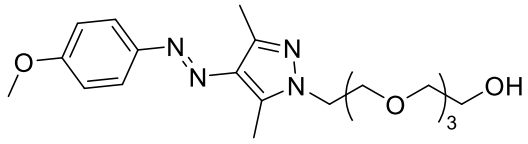

Yield: 7.40 g (18.2 mmol, 93 %) as orange oil.
^{1}H NMR (300 MHz, CDCl3): δ = 7.77 (m, 2H, CH), 6.96 (m, 2H, CH), 4.20 (t, *J*HH = 5.5 Hz, 2H, CH2), 3.86 (t, *J*HH = 5.5 Hz, 2H, CH2), 3.69 (m, 4H, CH2), 3.59 (m, 10H, CH2), 2.59 (s, 3H, CH3), 2.56 (s, 3H, CH3), 2.48 (s, 3H, CH3).
^{13}C-NMR (101MHz, $CDCl_3$)): δ =160.76, 147.93, 142.33, 139.51, 134.75, 123.29, 114.06, 77.48, 77.16, 76.84, 72.60, 70.69, 70.57, 70.48, 70.27, 69.90, 61.59, 55.53, 48.93, 14.01, 9.89.
ESI-HRMS (MeOH) (m/z): Calculated for $[C_{20}H_{30}N_4O_5Na]^+$: 429.2108, found: 429.2114.

AAP-3

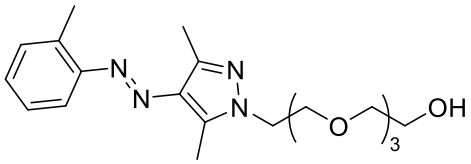

Yield: 4.03 g (10.32 mmol, 49 %) as orange oil.
^{1}H NMR (300 MHz, $CDCl_3$): δ = 7.60 – 7.11 (m, 4H), 4.15 (t, J = 5.4 Hz, 2H), 3.81 (t, J = 5.4 Hz, 2H), 3.70 - 3.60 (m, 2H), 3.60 – 3.42 (m, 4H), 3.51 (s, 5H), 3.38 (s, 1H), 2.58 (s, 3H), 2.57 (s, 3H), 2.46 (s, 3H).
^{13}C-NMR (101MHz, $CDCl_3$): δ = 151.65, 142.17, 140.60, 136.67, 135.74, 131.05, 129.32, 126.33, 114.69, 72.59, 70.76, 70.65, 70.57, 70.36, 69.96, 61.68, 49.07, 17.87, 14.44, 9.92.
ESI-HRMS (MeOH) (m/z): Calculated for $[C_{20}H_{30}N_4O_4Na]^+$: 413.2159, found: 413.2181.

AAP-4

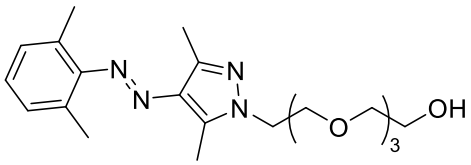

Yield: 0.73 g (1.80 mmol, 41 %) as red oil.
^{1}H NMR (400 MHz, $CDCl_3$): δ = 7.14 – 7.03 (m, 3H), 4.23 (t, J = 5.5 Hz, 2H), 3.89 (t, J = 5.5 Hz, 2H), 3.73 – 3.68 (m, 2H), 3.66 – 3.53 (m, 10H), 2.58 (s, 3H), 2.47 (s, 3H), 2.35 (s, 6H).
^{13}C-NMR (101MHz, $CDCl_3$): δ = 151.91, 141.77, 140.48, 135.63, 130.47, 129.15, 128.84, 127.15, 126.68, 77.48, 77.16, 76.84, 72.59, 70.73, 70.65, 70.57, 70.34, 69.96, 61.67, 49.01, 19.39, 18.35, 14.34, 9.84.

ESI-HRMS (MeOH) (m/z): Calculated for $[C_{21}H_{32}N_4O_4Na]^+$: 427.23158, found: 427.23178.

2. UV-Vis Absorption Spectra

UV/Vis absorption spectra over one cycle are shown below. Additionally, the absorbance at the absorption maximum for the *E*-Isomer is shown over five switching cycles to show reversible switching. All spectra were recorded in H_2O (c = 50 µM) and measured against the same solvent. Irradiation time were three to five min with UV light (365 nm) and green light (520 nm).

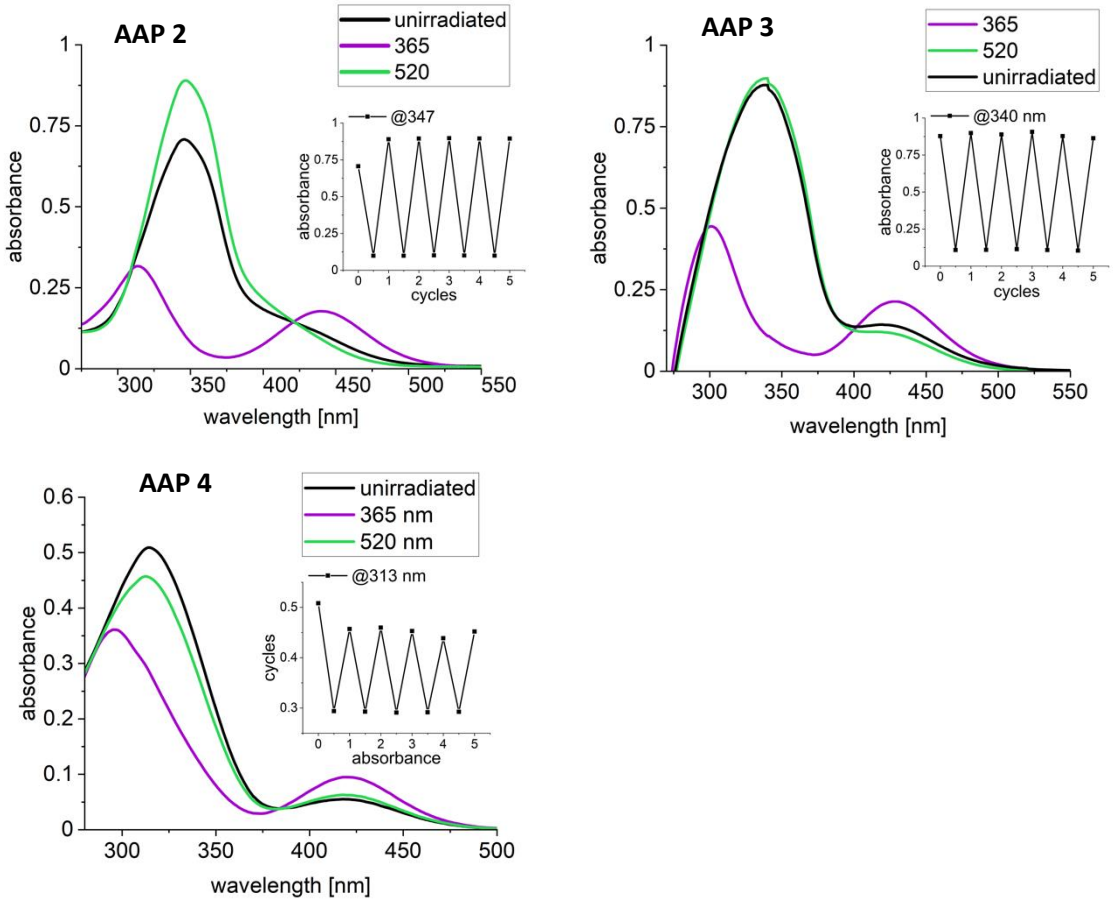

Figure S1: UV/vis-measurements of AAP-2 (top-left), AAP-3 (top-right), AAP-4 (bottom-left). Experimental spectrum of the photoisomerization in water and absorbance at 313 nm (AAP 4), 340 nm (AAP 3) and 347 nm (AAP 2) of five switching cycles.

3. Determination of photostationary states (PSS)

To determine the photostationary state (PSS) for the isomerization process from *E*→*Z* and *Z*→*E*, 1H-NMR spectroscopy was utilized. Therefore, a solution of AAP was prepared in D_2O (c = 200 µM). The initial spectrum was recorded, followed by irradiation with UV-light (365 nm) for 30 minutes to reach PSS *E*-*Z*. A second spectrum was then recorded. After irradiation with green light (530 nm, 30 min), the final spectrum at PSS *Z*-*E* was recorded. By integrating the proton signals in the methyl groups at the pyrazole, the ratio between both isomers at the photostationary states was determined. All NMR spectra and zoom-ins of the specific region used for determining the PSS are presented below.

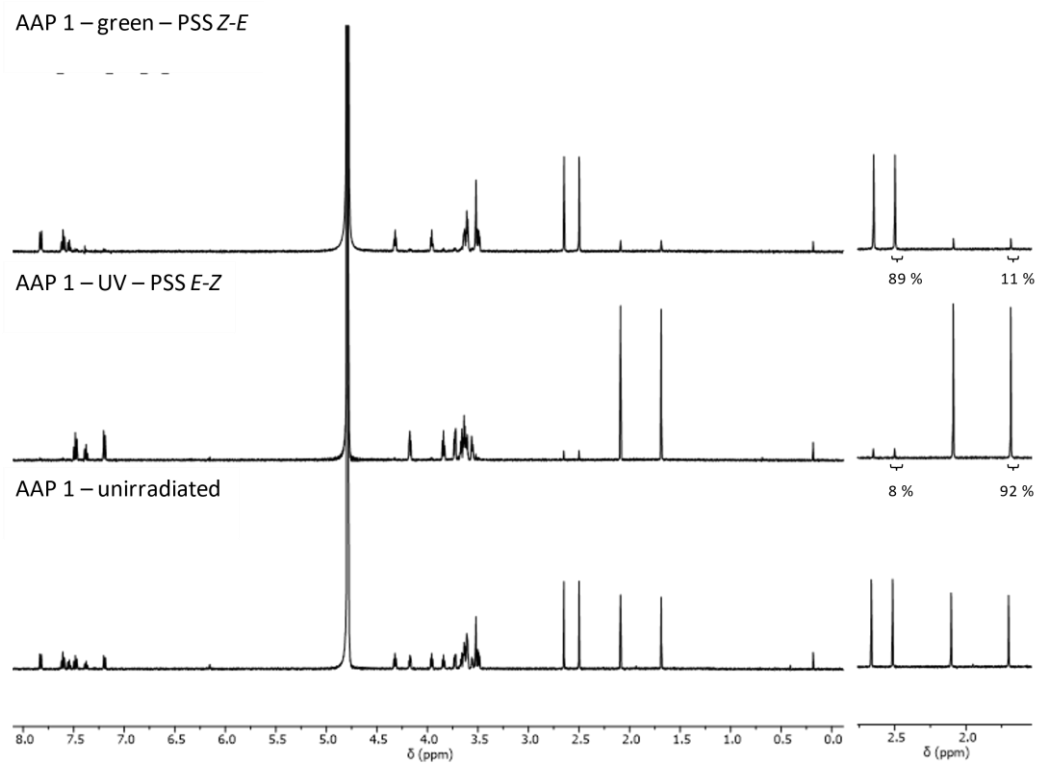

Figure S2: ^{1}H-NMR spectra for PSS determination of AAP-1.

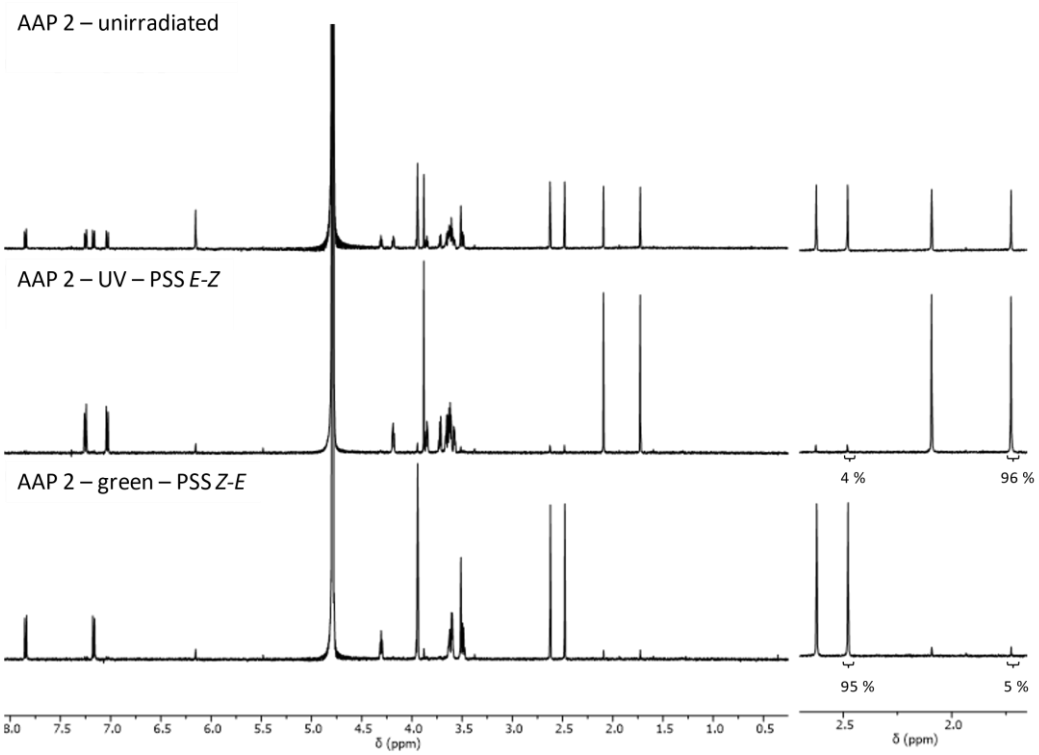

Figure S3: ^{1}H-NMR spectra for PSS determination of AAP-2.

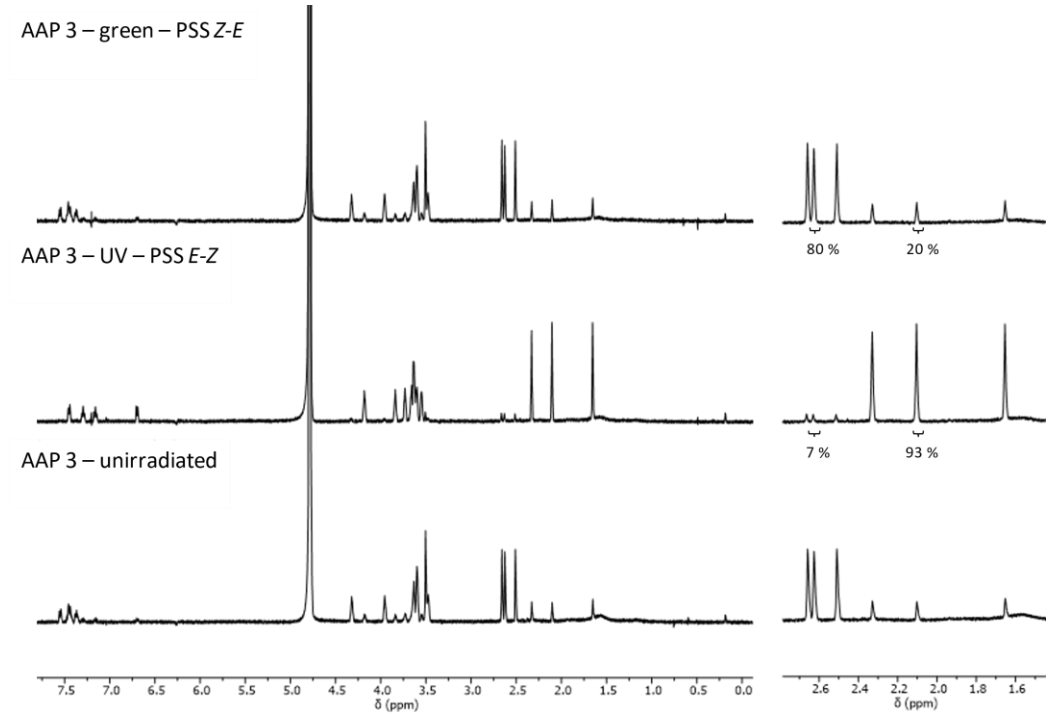

Figure S4: ^{1}H-NMR spectra for PSS determination of AAP-3**.**

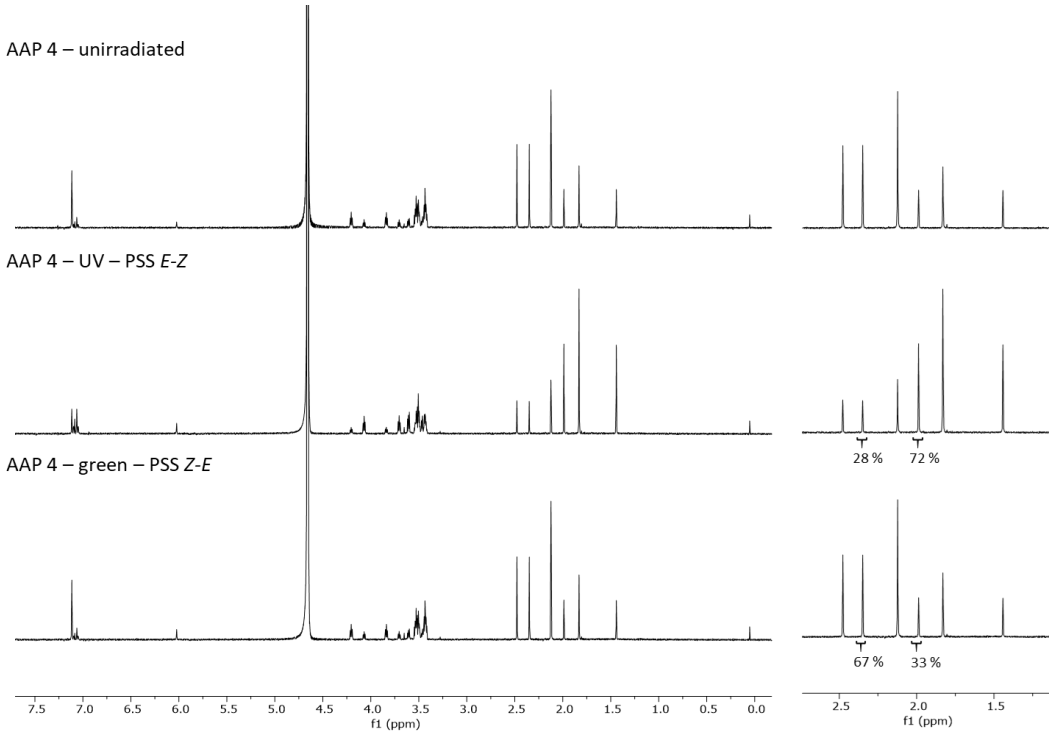

Figure S5: ^{1}H-NMR spectra for PSS determination of AAP-4.

4. Supplementary Transient Absorption Data

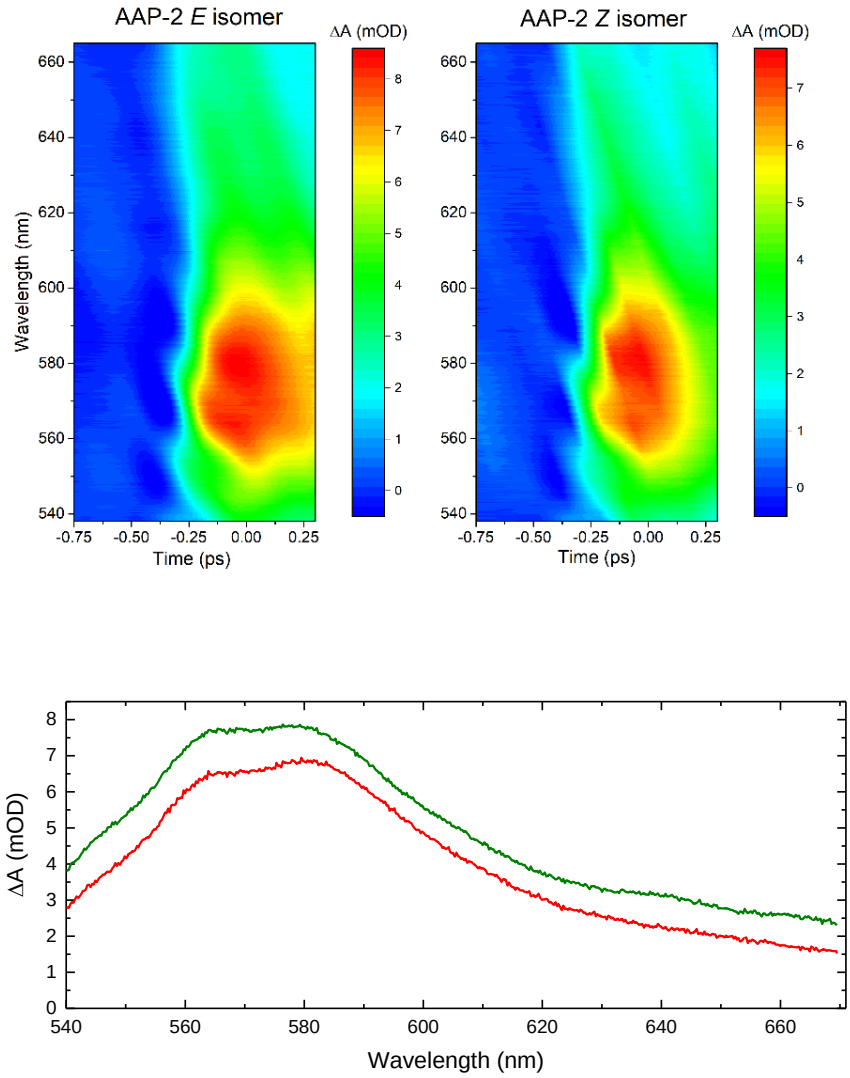

Figure S6: Transient absorption spectra (λ_{pump} =430 nm, λ_{probe} =490-900 nm) of *E*-AAP-2(left) and *Z*-AAP-2 (right) from 540-660 nm. The excited state absorption (ESA) is centered at 575 nm. The white-light probe was directly generated from our Yb:KGW laser (1030 nm, pulse duration: 200 fs) using a sapphire plate. The lower graph depicts the transient absorption spectrum at t = 0 fs for the *E*-isomer (green) and *Z*-isomer (red).

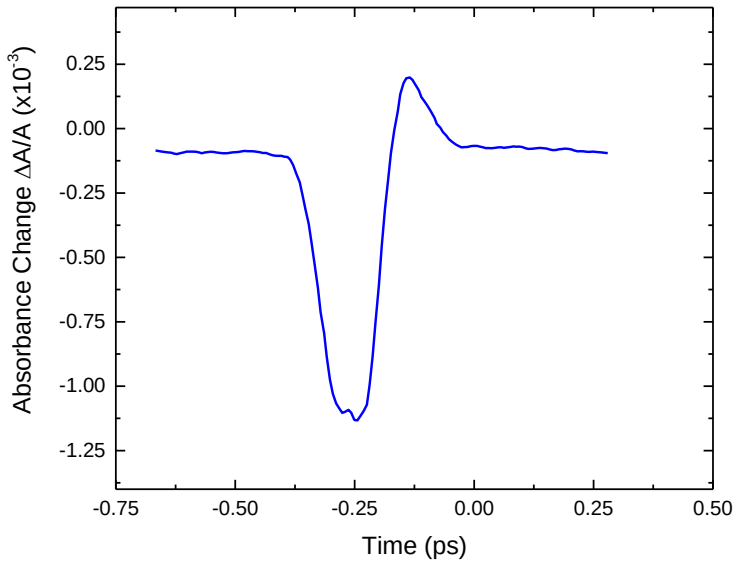

Figure S7: Pump-probe signal from water (λ_{pump} = 430 nm, λ_{probe} = 650 nm) displaying a negative cross-phase modulation signal before t=0.

5. Theoretical studies

5.1 Computational Details

Geometry optimizations and minimum energy path (MEP) calculations were executed with the Gaussian 16 Rev. B.01 package[2] employing the B3LYP hybrid functional[3] in conjunction with the 6-31G* basis set[4,5]. The standard convergence criteria for geometry optimizations and single point calculations were used, along with the addition of empirical dispersion correction of type Grimme D3 with Becke-Johnson damping[5–7]. To include solvent effects into the calculations, the polarizable continuum model (PCM)[8] for water was used and the cavity for the molecule was formed based on the UFF model for atomic radii[9]. For the visualization of molecular geometries and orbitals, VMD 1.9.3 with the internal Tachyon renderer was used.[10] Car-Parrinello molecular dynamics (MD) simulations in the gas phase were performed starting from the optimized structures to sample the rotational fluctuations of the ring systems attached to the azo moiety in the gas phase at 300 K using version 4.1 of CPMD.[11] Here, a cubic unit cell of size 18 Å was chosen (such that periodically repeated molecules are separated by at least 6 Å of vacuum), in conjunction with the PBE functional[12,13], a plane-wave basis truncated at 70 Ry, and norm-conserving Goedecker-type pseudopotentials[14] for the core-electrons; a time step of 4 au (0.0967 fs) was used together with a fictitious electron mass of 800 au and a Nosé-Hoover chain thermostat. Additional CP-MD runs employing the restricted open-shell Kohn-Sham (ROKS) ansatz[15] were done in order to probe the escape from the Franck-Condon region in the first excited electronic state with zero initial velocities. Using the ORCA software[16], we were also able to simulate the photoisomerization in the T_1 state employing the B3LYP hybrid functional with Grimme's D3 correction taking into account the water solvent by a PCM model. The T_1 state was calculated by Kohn-Sham DFT with multiplicity 3. For all photoisomerization runs, the initial velocities were set to zero and no thermostat was used.

The electronic structure of the π-systems involved in this work has been further analyzed by means of the Wiberg bond indices[16], as provided by the NBO population analysis[17] of the Gaussian16 package via the '$nbo bndidx $end' keyword.

UV/vis spectra were calculated at the TDDFT level of theory (PCM/GD3BJ/B3LYP/6-31G*). Transition dipole moments and oscillator strengths of the excited state absorption (ESA) of the S_1 state were calculated from the Gaussian TDDFT data employing the MultiWFN software package.

5.2 Optimized geometries

Table S1: Relative DFT energies (PCM/GD3BJ/B3LYP/6-31G*) and characteristic dihedral angles of the optimized structures of AAP-1, AAP-2, AAP-3, and AAP-4. Values in parentheses correspond to a flip of the asymmetric 5-membered pyrazole ring.

		dihedral angle°		
	energy/eV	azo unit	6-ring	5-ring
E:				
AAP-1	0.0 (0.053)	180.1 (180)	0.2 (0)	0.2 (180)
AAP-2	0.0 (0.053)	180.0 (180)	0.1 (0)	0.1 (180)
AAP-3	0.0 (0.049)	179.9 (180)	179.7 (180)	0.2 (180)
	0.103 (0.149)	180.2 (180.3)	5.0 (7.5)	0.0 (180.3)
AAP-4	0.0 (0.047)	181.2 (180.8)	27.9 (21.9)	1 (177.8)

Z:				
AAP-1	0.494 (0.517)	11.5 (10.6)	49.4 (49.0)	39.8 (-147.6)
AAP-2	0.512 (0.534)	12.0 (11.0)	45.0 (44.6)	42.8 (-146.3)
AAP-3	0.456 (0.480)	12.0 (9.3)	-137.8 (58.7)	39.2 (36.1)
	0.480 (0.502)	11.2 (8.4)	-137.8 (58.0)	-148.6 (-147.4)
AAP-4	0.328 (0.352)	9.3 (8.5)	60.5 (59.4)	34.5 (-148.4)

5.3 UV/vis absorption spectra

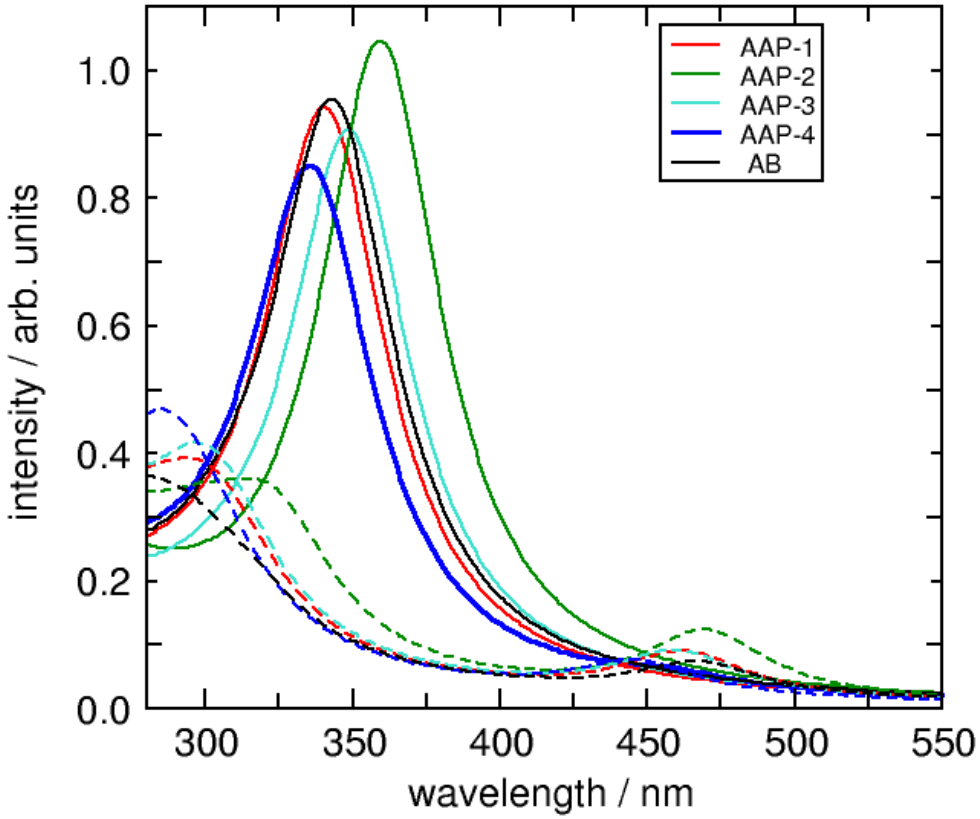

Figure S8: UV/vis absorption spectra (TDDFT, PCM/GD3BJ/B3LYP/6-31G*) of the optimized structures of AAP-1, AAP-2, AAP-3, and AAP-4. Solid lines: *E* conformer, dashed lines *Z* conformer. Data for azobenzene (AB) is shown as reference. Note: apart from AAP-4, the oscillator strength of the nπ*-excitation (S_1) is equal to zero due to the planar structure of the optimized compounds.

5.4 Excited state absorption and normal modes

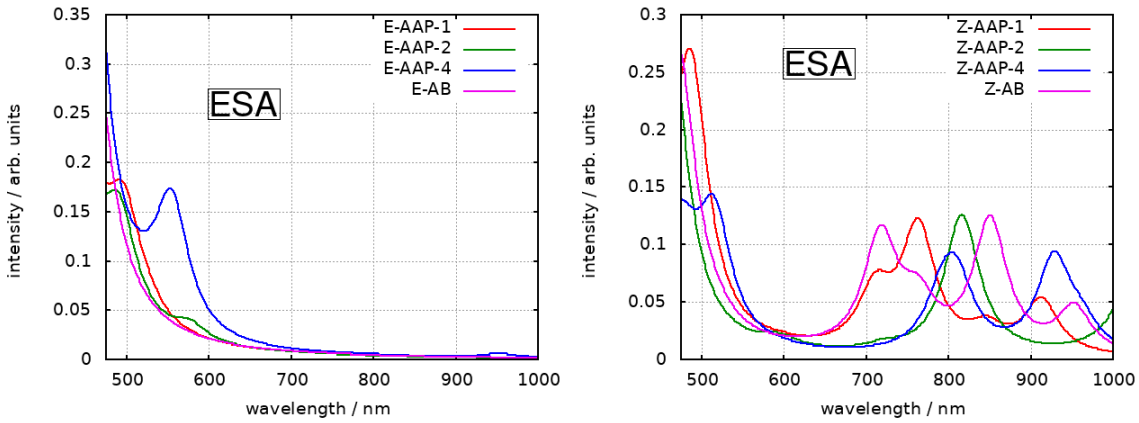

Figure S9: S1 ESA spectra (TDDFT, PCM/GD3BJ/B3LYP/6-31G*) of the optimized structures of AAP-1, AAP-2, AAP-3, and AAP-4. Left: *E* conformer, right: *Z* conformer. Data for azobenzene (AB) is shown as reference. Note: the band at about 560 nm corresponds to the S_1->S_5 excitation and is of weak oscillator strength for the planar structures.

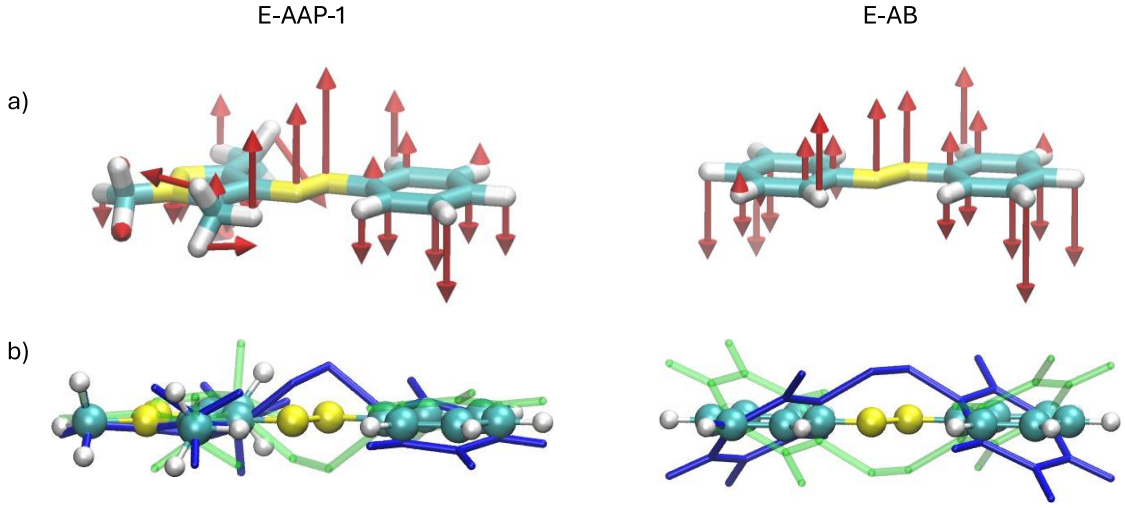

Figure S10: Visualization of the normal mode corresponding to the first negative eigenvalue of the Hessian calculated in the S_1 state for the S_0 minimum structure (Franck-Condon vertical excitation). a) Optimized structures in licorice representation with force vectors. b) Optimized structures in ball-and-stick representation together with the two turning point structures in blue and green stick representation, respectively.

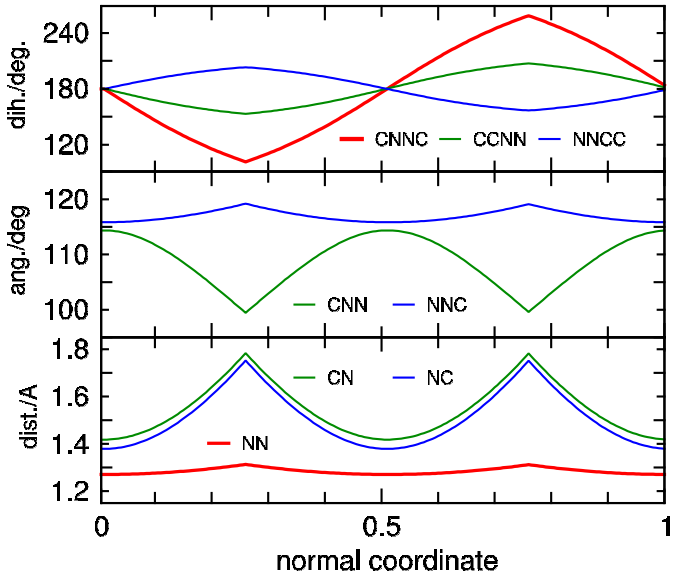

Figure S11: AAP-1: variation of bond angles, bond lengths and dihedral angles of the azo moiety along the normal mode coordinate shown in Fig. S10 for one vibrational period.

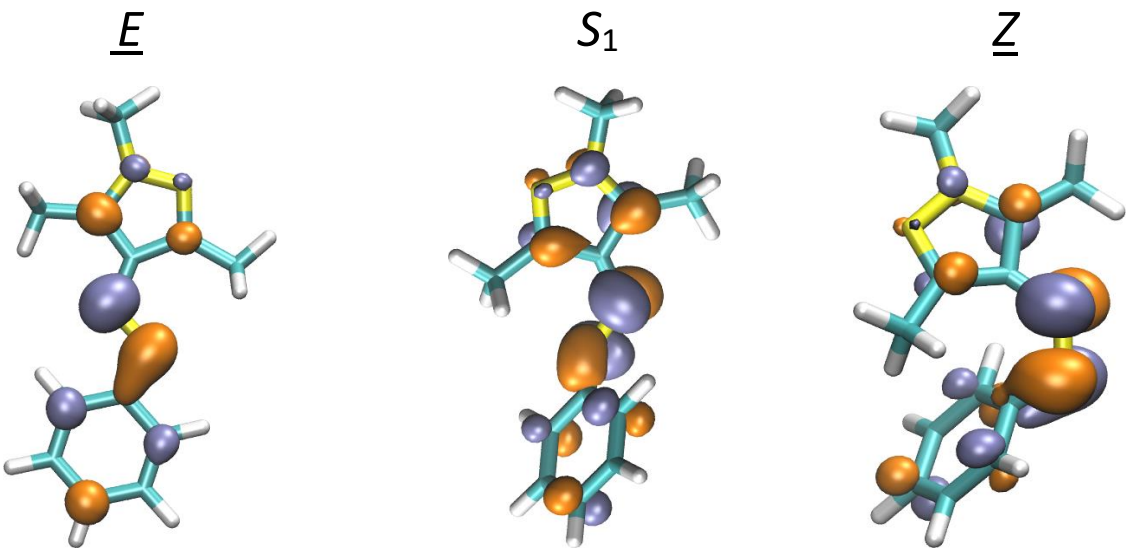

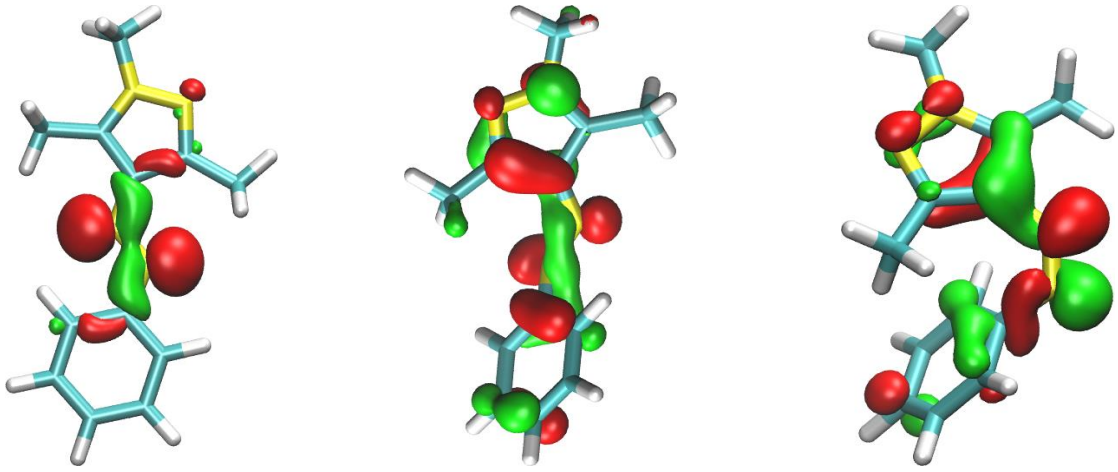

Figure S12: AAP-1: view of frontier molecular orbitals π* (top row) and n (bottom row) at *E* (left) and *Z* (right) ground state minima and S_1 relaxed structure (middle). Contours are shown at an iso value of 0.05.

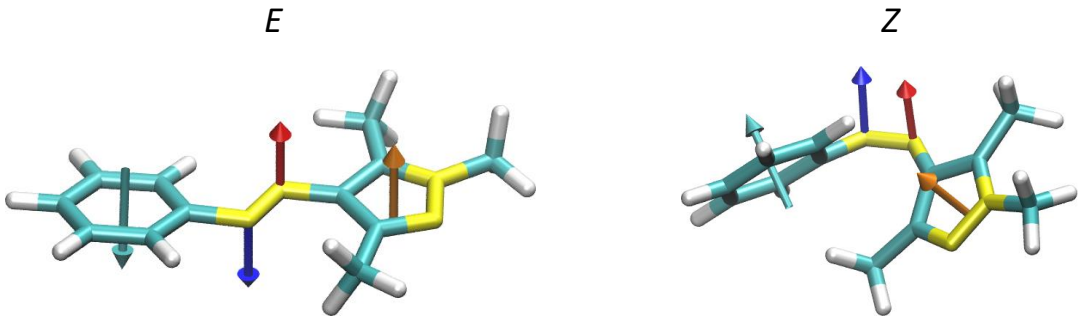

Figure S13: AAP-1: plane normal vectors of azo group (blue, red) and attached ring systems (cyan, orange) indicating the relative orientation of their π systems. Left: *E*-AAP-1, right: *Z*-AAP-1.

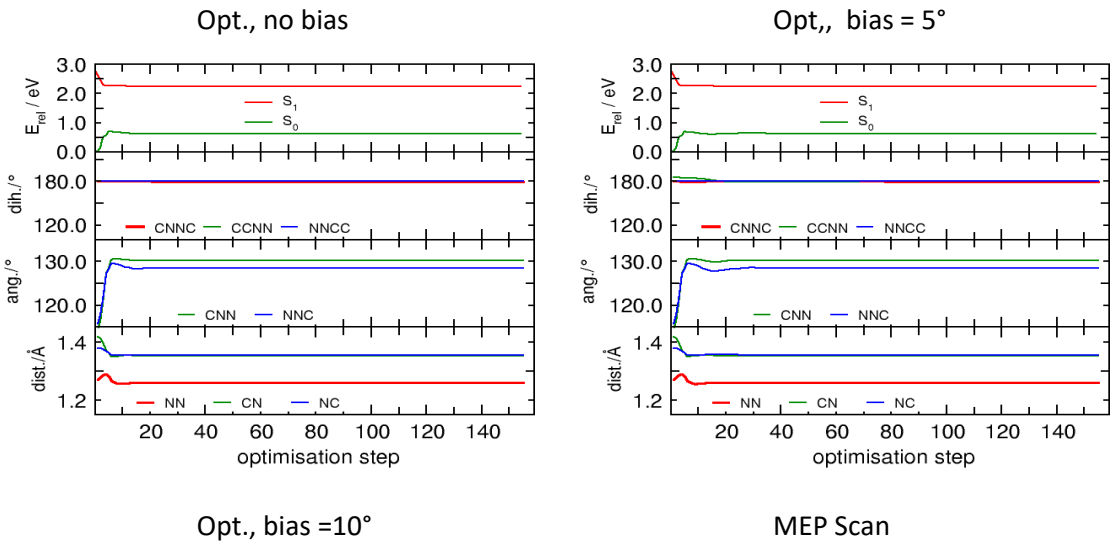

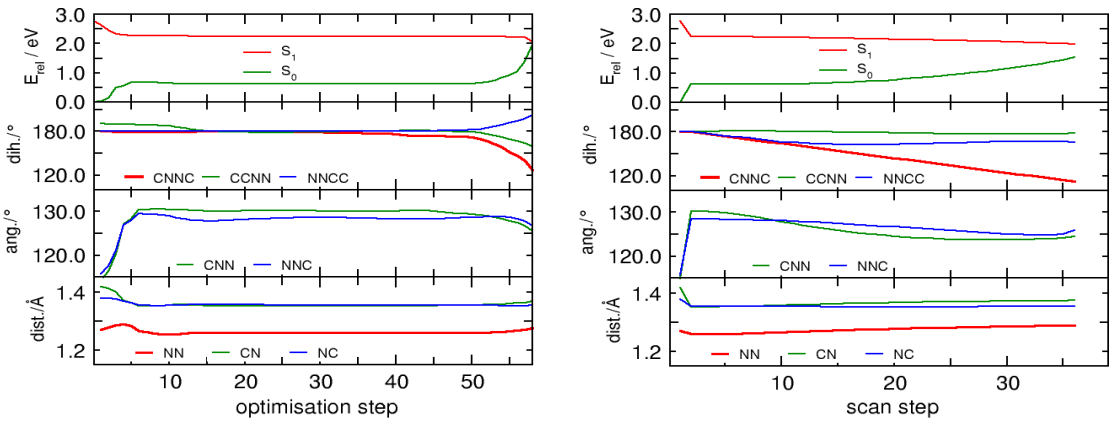

Figure S14: AAP-1: escape from the Franck-Condon region in the S_1 state probed by steepest descent geometry optimisation and (bottom right) MEP scan along the CNNC internal coordinate. Geometry optimisation calculations were started with S_0 minimum structure (top left) and increasing out-of-plane rotation bias of the phenyl ring (top right: 5°, bottom left: 10°).

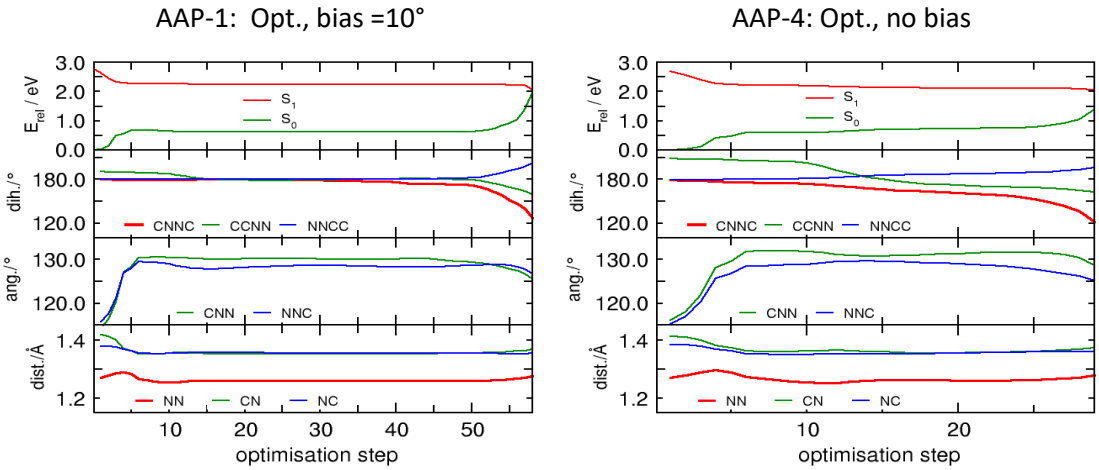

Figure S15: Comparison of AAP-1 and AAP-4: escape from the Franck-Condon region in the S_1 state probed by steepest descent geometry optimisation (see also Fig. S14).

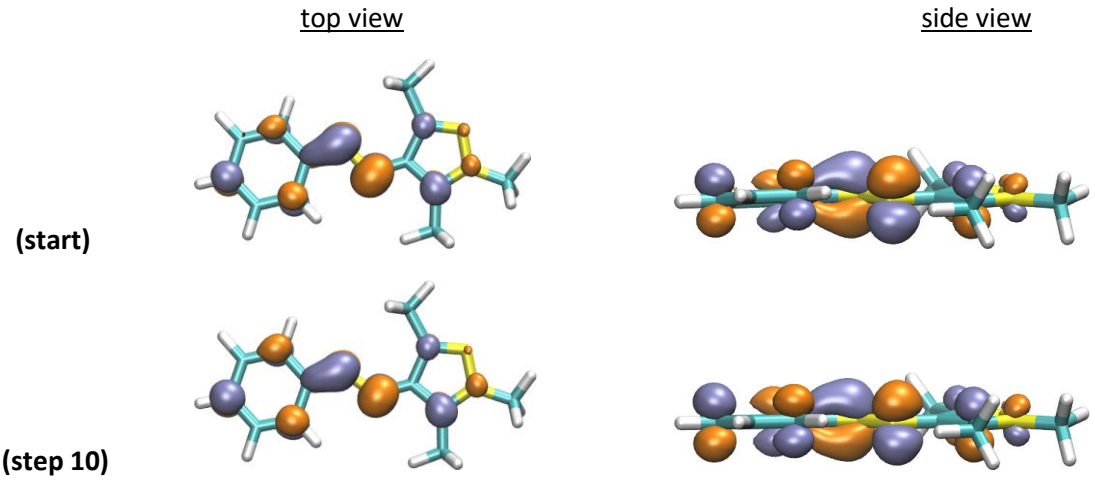

(step 52)

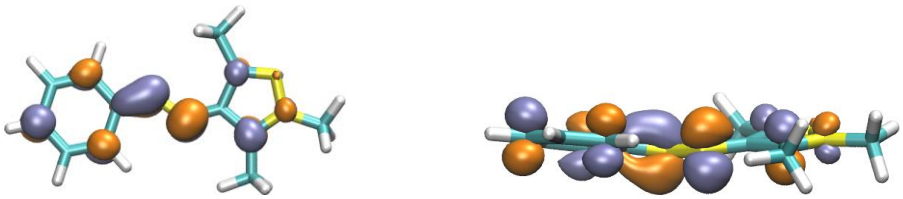

(step 54)

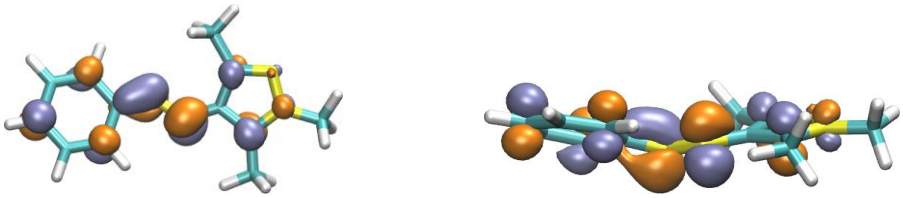

(step 56)

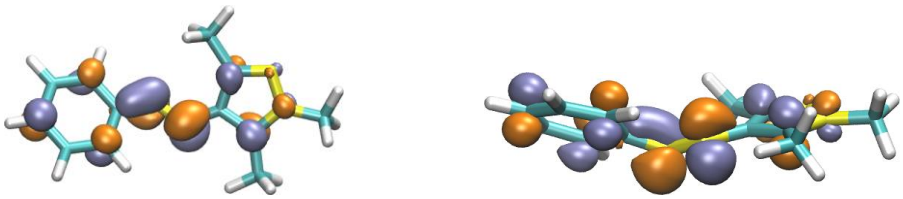

(step 57)

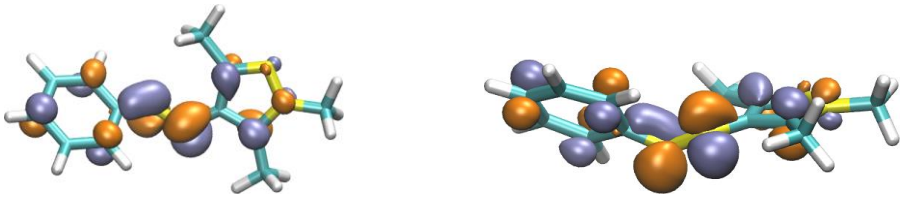

(step 58)

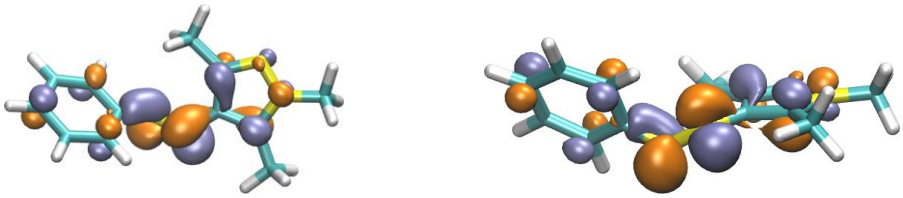

Figure S16: AAP-1: top view (left column) and side view (right column) of the π* orbital (LUMO) in course of S_1 geomtery optimisation (cf. Fig.13, bottom left).

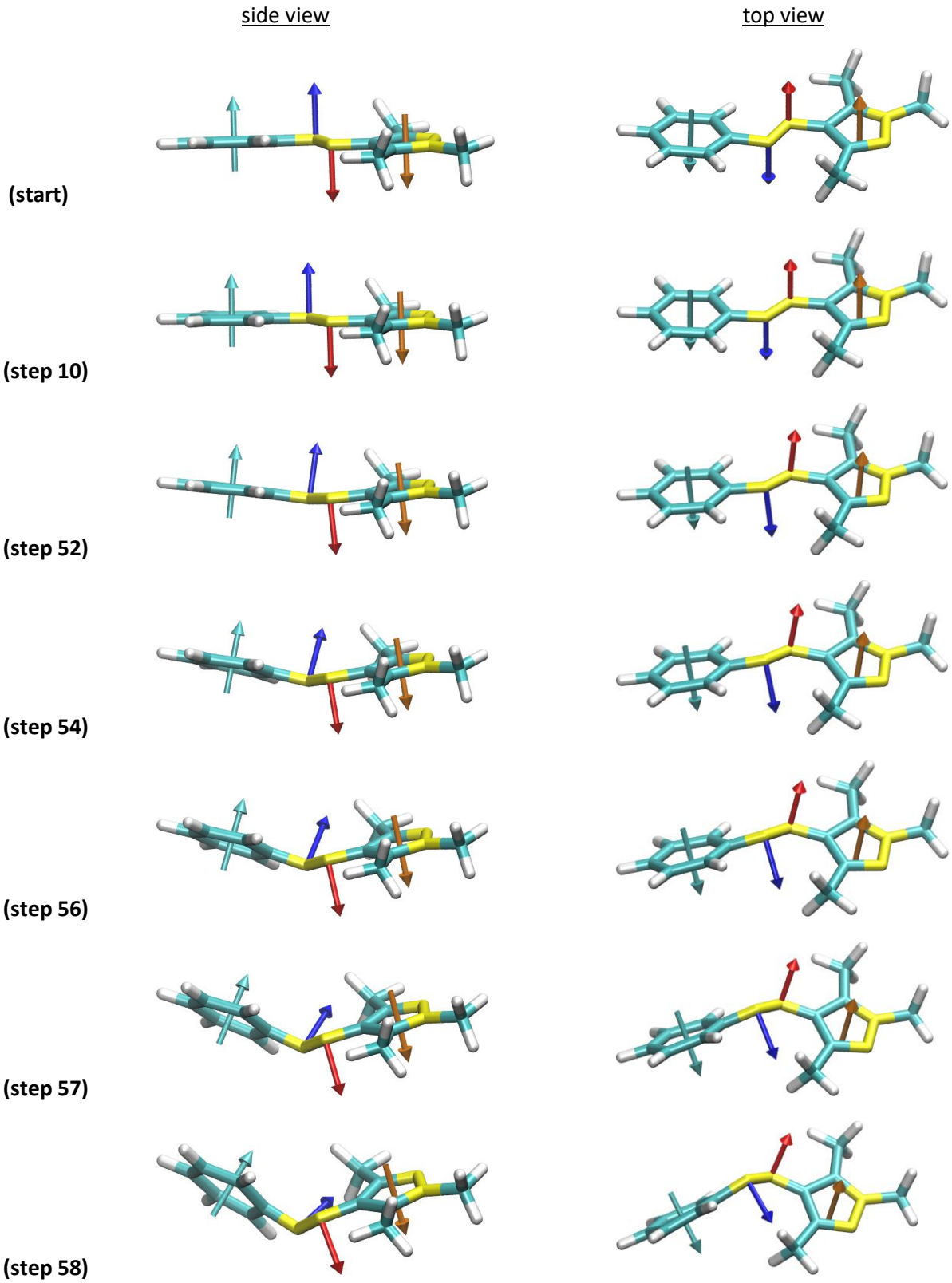

Figure S17: AAP-1: plane normal vectors of azo group (blue, red) and attached ring systems (cyan, orange) indicating the relative orientation of their π systems in course of S_1 geometry optimisation (cf. Fig. S14, bottom left).

5.5 Ground state dynamics

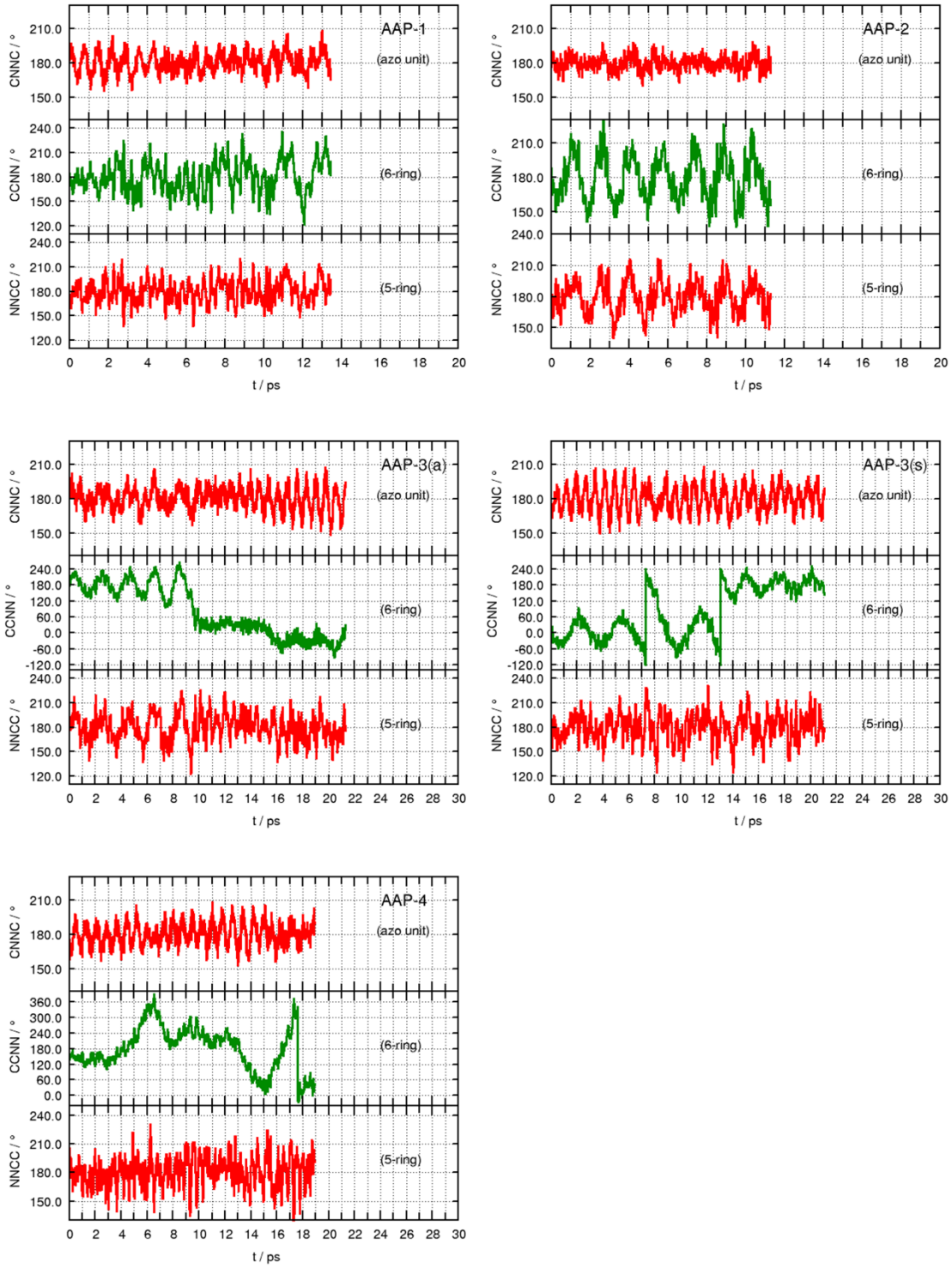

Figure S18: Time evolution of selected dihedral angles obtained from ground state Car-Parrinello MD at 300 K starting in the minima of the AAPs.

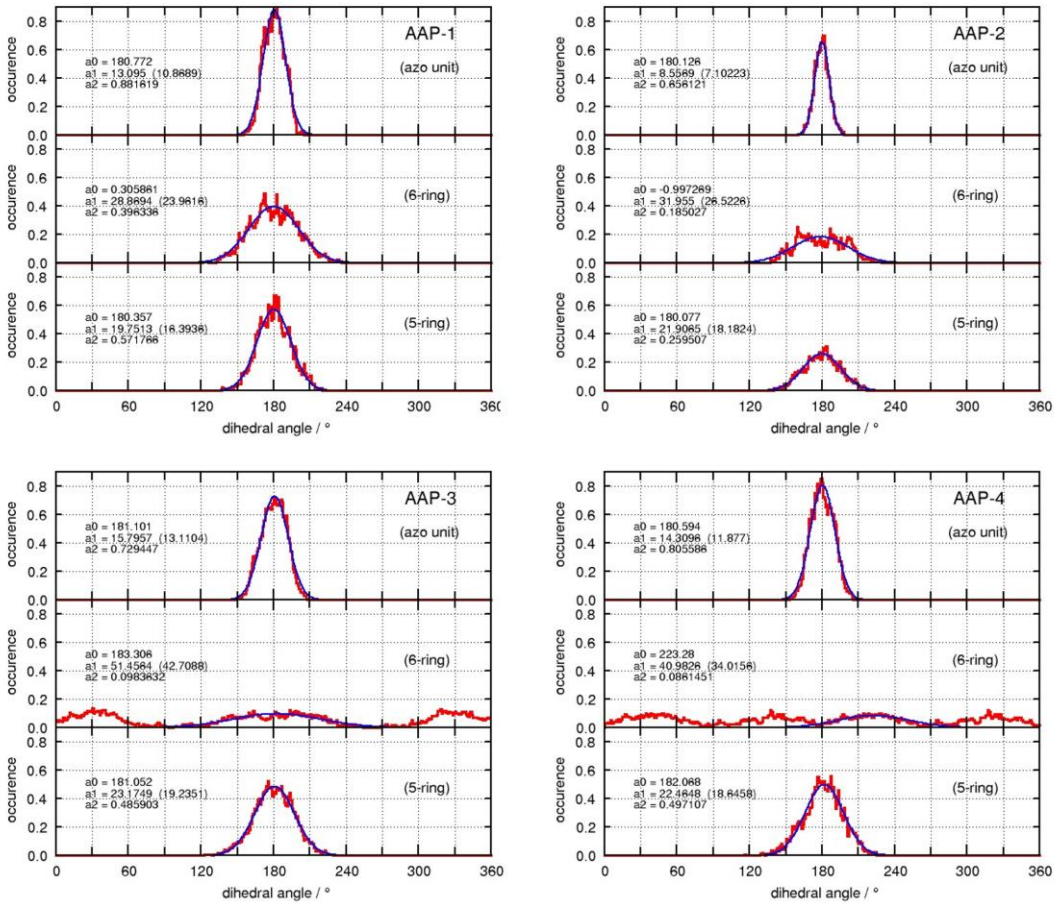

Figure S19: Histograms of the ground state MD trajectories of Figure S18. Data for AAP-3 has been unified, data for AAP-4 has been symmetrized. A fit to a Gauss function with center a_0, width a_1, and height a_2 was performed in the individual cases (blue).

5.6 Molecular orbital analysis

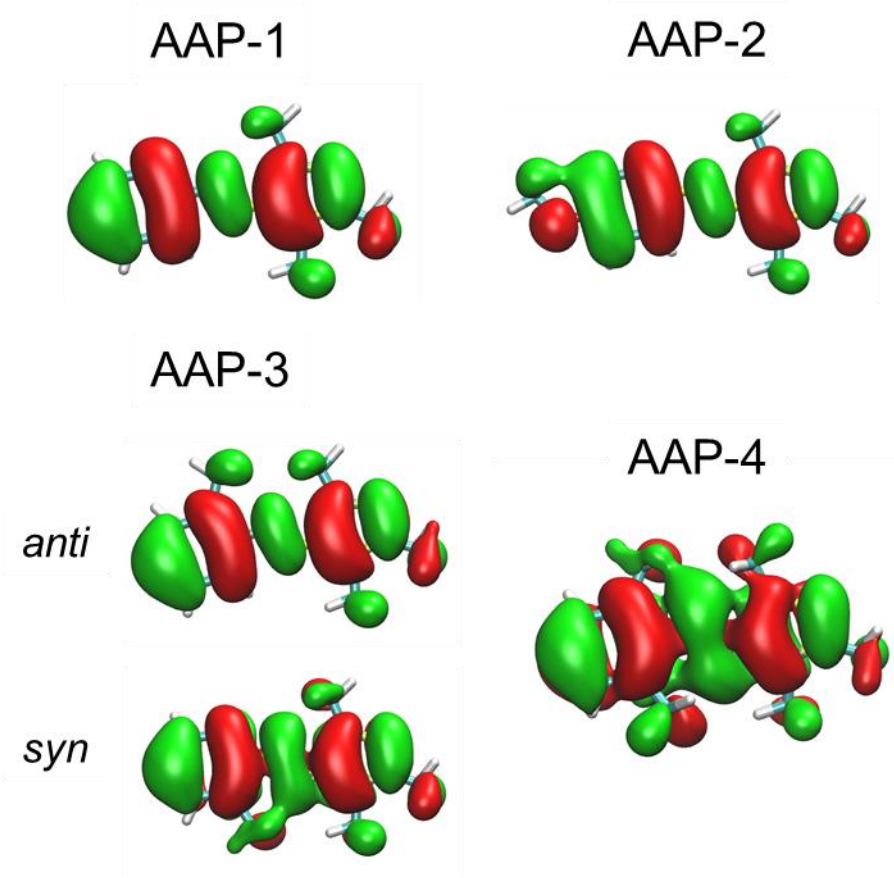

Figure S20: Frontier molecular orbitals (HOMO) of the different AAPs characterizing the extension of the π-system. Contours are shown at an iso value of 0.01.

5.7 Wiberg bond indices

The data compiled in Table S2 (including butadiene as a reference) shows that the corresponding bond matrix element is quite indicative of the degree of delocalisation of formal double bonds. Out-of-plane rotation of the respective ring system diminishes the conjugation with the azo chromophore (cf. Fig. S21, top row: green and blue curves (phenyl), green and black curves (pyrazole)), and the ring system bonds adopt values according to the isolated species when oriented orthogonal to the azo unit (cf. Table S2). The interaction of the two ortho-methyl groups with the two nitrogen atoms of the chromophore unit is seen to be much more pronounced for the phenyl ring than for the pyrazole ring (Fig. S21, bottom row), corresponding to a lower energy barrier.

Comparison of the data for AAP-1 and AAP-4 reveals that the (’through space’) interaction of the ortho methyl groups pertains for AAP-4, on average, throughout the out-of-plane rotation (cf. Fig. S22, left), while the corresponding data for AAP-1 and AAP-2 is rather similar (cf. Fig. S22, right), showing a decreasing progression.

Table S2: Comparison of conjugated π-systems: Wiberg bond indices for the relevant basic structures. In delocalized π-systems, the Wiberg indices adopt values between 1 (ideal single bond) and 2 (ideal double bond).

	bond							
structure	1–2	2–3	3–4	4–5	5–6	6–1	1–12	12–13
linear:								
no conjugation	2	1	2					
butadiene, anti (180°)	1.8838	1.1250	1.8838	-	-	-	-	-
butadiene, perpend. (100°)	1.9872	1.0297	1.9872	-	-	-	-	-
butadiene, gauche (30°)	1.9135	1.0938	1.9135	-	-	-	-	-
6-ring:								
no conjugation	2	1	2	1	2	1		
benzene	1.4366	1.4365	1.4366	1.4365	1.4366	1.4365	-	-
1,3-dimethyl-benzene	1.4104	1.4104	1.4023	1.4365	1.4364	1.4024	-	-
methoxy-benzene	1.3538	1.4690	1.4080	1.4507	1.4195	1.3838	1.0065	0.9123
5-ring:								
no conjugation	2	1	1	2	1			
2,5-dimethyl-pyrazole	1.4871	1.2140	1.1820	1.4980	1.3300	-	-	-

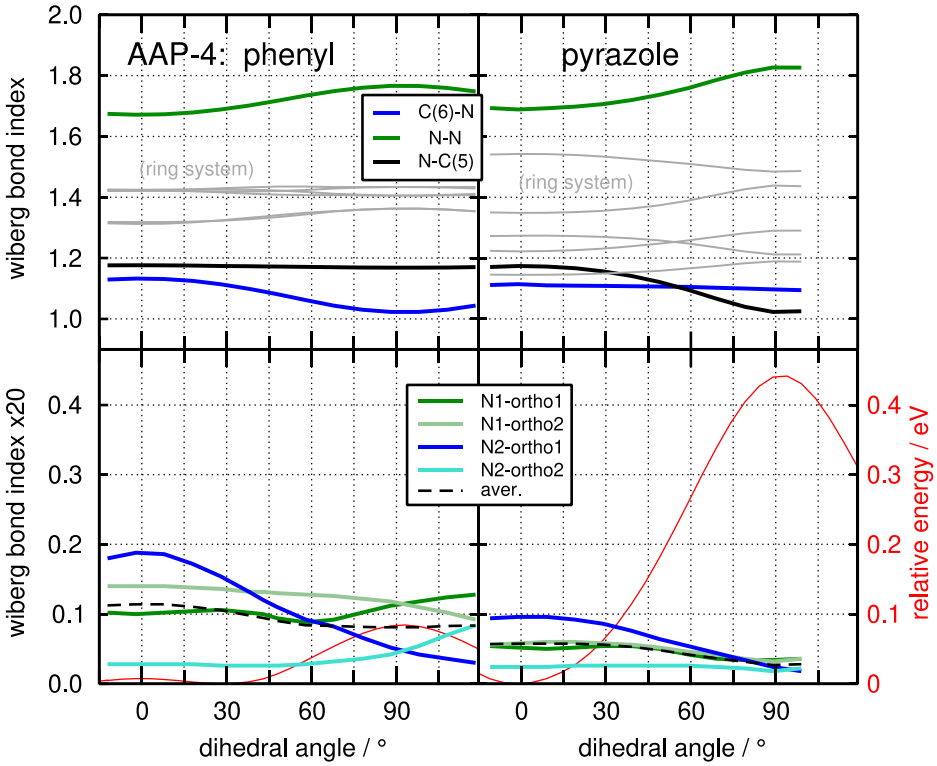

Figure S21: Comparison of Wiberg bond index values of AAP-4 as a function of the dihedral angle of the (left) phenyl ring and (right) pyrazole ring attached to the azo unit. Top row displays curves for the three bonds of the central azo unit (bonds of the ring systems are shown in grey for sake of completeness), bottom row displays corresponding values for the interaction of the ortho-methyl groups with the two nitrogen atoms of the azo unit; the red curves display the rotational energy barrier as a reference and orientation to the reader.

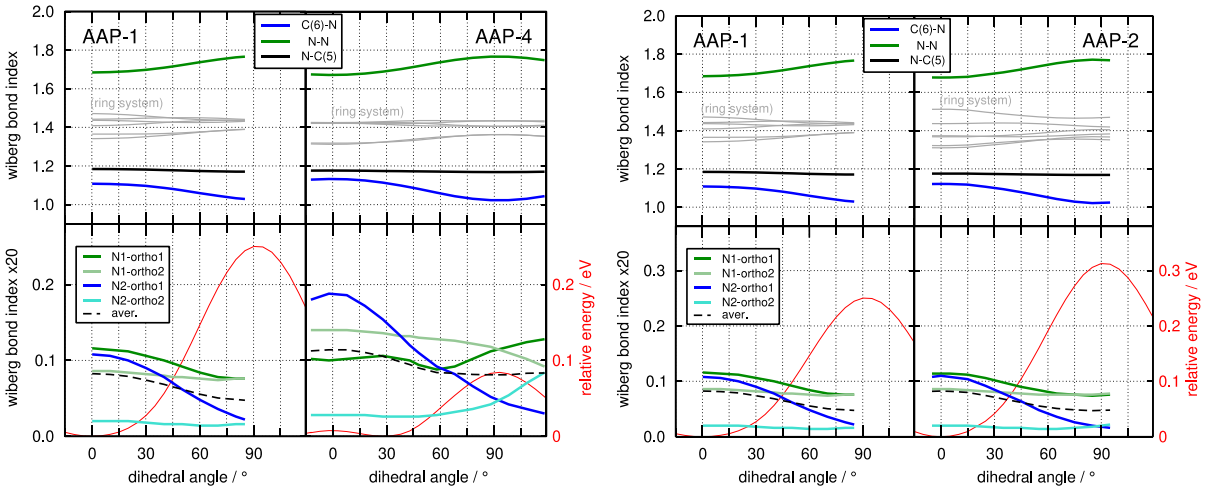

Figure S22: Comparison of Wiberg bond index values of (left) AAP-1 and AAP-4 and (right) AAP-1 and AAP-2 as a function of the dihedral angle of the phenyl ring attached to the azo unit. Top row displays curves for the three bonds of the central azo unit (bonds of the ring systems are shown in grey for sake of completeness), bottom row displays corresponding values for the interaction of the ortho-methyl groups with the two nitrogren atoms of the azo unit; the red curves display the rotational energy barrier as a reference and orientation to the reader.

5.8 Photoisomerisation dynamics

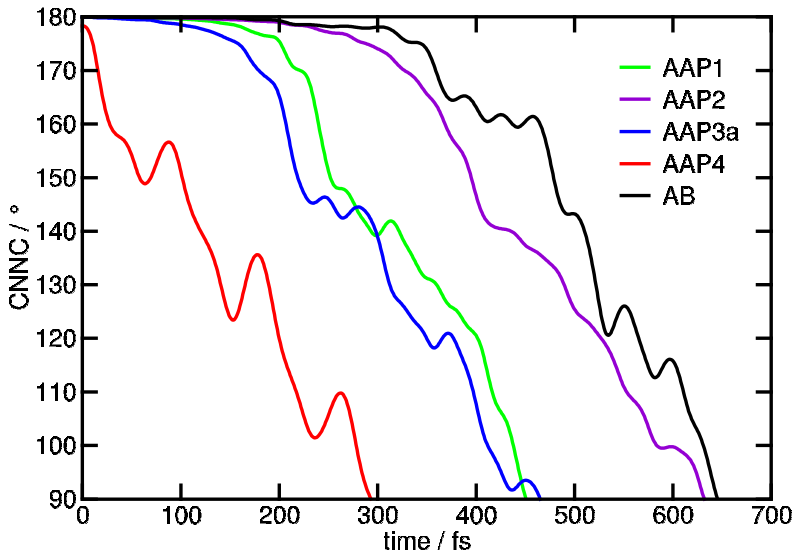

Figure S23: CNNC angle as a function of time for the E isomers of the different AAPs compared to AB obtained from MD simulations in the T_1 state in water.

References

(1) Stricker, L., Böckmann, M., Kirse, T. M., Doltsinis, N. L., Ravoo, B. J. Arylazopyrazole Photoswitches in Aqueous Solution: Substituent Effects, Photophysical Properties, and Host-Guest Chemistry. *Chem. Eur. J.* **2018**, *24*, 8639–8647.

(2) M. J. Frisch, G. W. Trucks, H. B. Schlegel, G. E. Scuseria, M. A. Robb, J. R. Cheeseman, G. Scalmani, V. Barone, G. A. Petersson, H. Nakatsuji, X. Li, M. Caricato, A. V. Marenich, J. Bloino, B. G. Janesko, R. Gomperts, B. Mennucci, H. P. Hratchian, J. V. Ortiz, A. F. Izmaylov, J. L. Sonnenberg, D. Williams-Young, F. Ding, F. Lipparini, F. Egidi, J. Goings, B. Peng, A. Petrone, T. Henderson, D. Ranasinghe, V. G. Zakrzewski, J. Gao, N. Rega, G. Zheng, W. Liang, M. Hada, M. Ehara, K. Toyota, R. Fukuda, J. Hasegawa, M. Ishida, T. Nakajima, Y. Honda, O. Kitao, H. Nakai, T. Vreven, K. Throssell, J. A. Montgomery, Jr., J. E. Peralta, F. Ogliaro, M. J. Bearpark, J. J. Heyd, E. N. Brothers, K. N. Kudin, V. N. Staroverov, T. A. Keith, R. Kobayashi, J. Normand, K. Raghavachari, A. P. Rendell, J. C. Burant, S. S. Iyengar, J. Tomasi, M. Cossi, J. M. Millam, M. Klene, C. Adamo, R. Cammi, J. W. Ochterski, R. L. Martin, K. Morokuma, O. Farkas, J. B. Foresman, and D. J. Fox. *Gaussian 16*: Wallingford CT, 2016.

(3) Stephens, P. J., Devlin, F. J., Chabalowski, C. F., Frisch, M. J. Ab Initio Calculation of Vibrational Absorption and Circular Dichroism Spectra Using Density Functional Force Fields. *J. Phys. Chem.* **1994**, *98*, 11623–11627.

(4) Francl, M. M., Pietro, W. J., Hehre, W. J., Binkley, J. S., Gordon, M. S., DeFrees, D. J., Pople, J. A. Self-consistent molecular orbital methods. XXIII. A polarization-type basis set for second-row elements. *J. Chem. Phys.* **1982**, *77*, 3654–3665.

(5) Smith, D. G. A., Burns, L. A., Patkowski, K., Sherrill, C. D. Revised Damping Parameters for the D3 Dispersion Correction to Density Functional Theory. *J. Phys. Chem. Lett.* **2016**, *7*, 2197–2203.

(6) Grimme, S., Ehrlich, S., Goerigk, L. Effect of the damping function in dispersion corrected density functional theory. *J. Comput. Chem.* **2011**, *32*, 1456–1465.
(7) Grimme, S., Antony, J., Ehrlich, S., Krieg, H. A consistent and accurate ab initio parametrization of density functional dispersion correction (DFT-D) for the 94 elements H-Pu. *J. Chem. Phys.* **2010**, *132*, 154104.
(8) Miertuš, S., Scrocco, E., Tomasi, J. Electrostatic interaction of a solute with a continuum. A direct utilizaion of AB initio molecular potentials for the prevision of solvent effects. *Chem.* **1981**, *55*, 117–129.
(9) Rappe, A. K., Casewit, C. J., Colwell, K. S., Goddard, W. A., Skiff, W. M. UFF, a full periodic table force field for molecular mechanics and molecular dynamics simulations. *J. Am. Chem. Soc.* **1992**, *114*, 10024–10035.
(10) Humphrey, W., Dalke, A., Schulten, K. VMD: visual molecular dynamics. *J. Mol. Graph.* **1996**, *14*, 33-8, 27-8.
(11) Hutter, J., Iannuzzi, M. CPMD: Car-Parrinello molecular dynamics. *Z. Kristallogr. – Cryst. Mater.* **2005**, *220*, 549–551.
(12) Perdew, J. P., Burke, K., Ernzerhof, M. Generalized Gradient Approximation Made Simple. *Phys. Rev. Lett.* **1996**, *77*, 3865–3868.
(13) Perdew, J. P., Burke, K., Ernzerhof, M. Generalized Gradient Approximation Made Simple. *Phys. Rev. Lett.* **1997**, *78*, 1396.
(14) Hartwigsen, C., Goedecker, S., Hutter, J. Relativistic separable dual-space Gaussian pseudopotentials from H to Rn. *Phys. Rev. B* **1998**, *58*, 3641–3662.
(15) Frank, I., Hutter, J., Marx, D., Parrinello, M. Molecular dynamics in low-spin excited states. *J. Chem. Phys.* **1998**, *108*, 4060–4069.
(16) Neese, F. Software update: The ORCA program system – Version 5.0. *WIREs Comput. Mol. Sci.* **2022**, 12, e1606. DOI:10.1002/wcms.1606.
(17) Wiberg, K. Application of the Pople-Santry-Segal CNDO method to the cyclopropyl-carbinyl and cyclobutyl cation and to bicyclobutane. *Tetrahedron*, **1968**, *24*, 1083-1096.
(18) Liu, T.and Chen. F. Multiwfn—A Multifuncional Wavefunction Analyzer. *J. Comput. Chem*, **2012**, *33*, 580-592.